

Modelling of Atherosclerotic Plaque for use in a Computational Test-Bed for Stent Angioplasty.

Conway, C., McGarry, J.P. and McHugh, P.E.

Biomechanics Research Centre (BMEC), Biomedical Engineering, College of Engineering and Informatics, National University of Ireland Galway, Galway, Ireland.

Abstract

A thorough understanding of the diseased tissue state is necessary for the successful treatment of a blocked arterial vessel using stent angioplasty. The constitutive representation of atherosclerotic tissue is of great interest to researchers and engineers using computational models to analyse stents, as it is this *in silico* environment that allows extensive exploration of tissue response to device implantation. This paper presents an *in silico* evaluation of the effects of variation of atherosclerotic tissue constitutive representation on tissue mechanical response during stent implantation. The motivation behind this work is to investigate the level of detail that is required when modelling atherosclerotic tissue in a stenting simulation, and to give recommendations to the FDA for their guideline document on coronary stent evaluation, and specifically the current requirements for computational stress analyses. This paper explores the effects of variation of the material model for the atherosclerotic tissue matrix, the effects of inclusion of calcifications and a lipid pool, and finally the effects of inclusion of the Mullins effect in the atherosclerotic tissue matrix, on tissue response in stenting simulations. Results indicate that the inclusion of the Mullins effect in a direct stenting simulation does not have a significant effect on the deformed shape of the tissue or the stress

state of the tissue. The inclusion of a lipid pool induces a local redistribution of lesion deformation for a soft surrounding matrix and the inclusion of a small volume of calcifications dramatically alters the local results for a soft surrounding matrix. One of the key findings from this work is that the underlying constitutive model (elasticity model) used for the atherosclerotic tissue is the dominant feature of the tissue representation in predicting tissue response in a stenting simulation.

Introduction

Atherosclerotic tissue is highly heterogeneous and can be comprised of a lipid core, calcifications, cellular debris, and fibrous tissue. However, the representation of atherosclerotic plaque tissue in computational stenting simulations has predominantly been as a homogeneous continuum, for example as presented in [1–8] and as most recently reviewed in [9]. Even though the analysis of angioplasty with stenting has been an area of intense interest to the computational biomechanics community in recent years [10], stenting simulations where the heterogeneous nature of the atherosclerotic tissue is explicitly represented are rare [10]. One study of note is that of Timmins et al. [8] where the stiffness of the plaque wall was varied with respect to the arterial stiffness. In addition to this work there has a small number of studies that do explicitly represent plaque substructure includes the work of Holzapfel *et al.* [11] where distinct lipid and calcified regions are represented in a patient specific model of coronary stent angioplasty; the work of García *et al.* [12] where models to assess self-expanding stent radial force are generated with lipid or calcified plaque cores; the work of Iannaccone *et al.* [10] where models with lipid pools and fibrous caps are generated to assess the effect of vascular anatomy on carotid stenting; and the work of Morlacchi *et al.* [13] where an assessment is made of the influence of large plaque calcifications on coronary stent fatigue life. Computational approaches to plaque modelling relevant to this application have recently been reviewed in Holzapfel *et al.* [14].

In conjunction with geometrical simplifications, the behaviour of atherosclerotic plaque tissue is generally considered to be hyperelastic and that it follows physiological behaviour (domain where blood pressure in arterial walls is less than 140 mmHg [15]), despite the fact that loading due to stent placement introduces supra-physiological forces (pressures above the physiological blood pressure) within the tissue.

This simplicity in constitutive representation is based on the fact that, relative to non-diseased (healthy) arterial tissue, and other widely studied bodily tissues such as bone for example, there is a distinct lack of comprehensive experimental data for the properties of atherosclerotic plaque tissue [16,17]. This lack of data can be due, amongst other factors, to the difficulty in obtaining, isolating and handing the tissue, the inherent variability and heterogeneity of the tissue, and the lack of a robust animal model that is representative of the disease in humans.

Where mechanical characterisation of atherosclerotic tissue has been addressed, the most common approach has been to view the tissue from a macroscopic continuum mechanics perspective, where the focus has not been on the mechanical characterisation of local plaque constituents, for example as presented in [18–25].

A smaller group of studies has focused on plaque tissue substructure mechanical characterisation, using a range of testing techniques. This includes the work of Holzapfel *et al.* [26] on plaque tissue component tensile testing; Lee *et al.* [27] who tested atherosclerotic plaque caps in cyclic compression; Loree *et al.* [28] who investigated the shear modulii of synthetic lipid pools; Ebenstein *et al.* [29] who used nano-indentation to investigate the mechanical properties of individual constituents; and Barrett *et al.* [30] and Chai *et al.* [31] who used micro-indentation to mechanically characterise atherosclerotic carotid plaque caps [31,32], and carotid intima and lipid cores [31]. Nano- and micro-indentation, while

presenting great potential for spatially resolving local tissue variations, are limited in the strain ranges that can be applied, which render them of limited use for characterising tissue behaviour in the high-strain supra-physiological domain relevant to the stenting application. In this context, data for mechanical (tensile) testing to rupture is particularly valuable [33]. More recently, Mulvihill *et al.* [34] reported tensile test data for non-calcified and calcified human carotid plaque tissue. For further information on atherosclerotic tissue testing, characterisation and relevant material properties, the reader is referred to the recent comprehensive review [16] and a “plaque mechanics” special issue [17] (in particular [14,33,35–37]).

Against this backdrop of limited experimental data, the primary aim of this work is to investigate the level of detail that is necessary and appropriate when modelling the response of atherosclerotic plaque tissue to stenting. It is hoped that the results will inform the choice and design of experiments necessary to adequately characterise the tissue for use in computational models. It will be confirmed (consistent with the observations above) that not only is further experimentation on atherosclerotic tissue required but also that knowledge of the tissue behaviour in failure is vital. An additional motivation for the present work is to provide recommendations to the FDA for the stress-strain analysis section of their guideline document on non-clinical engineering tests for coronary stents [38] for modelling the physiological environment.

Specifically, a 50% stenosed three layer arterial model is used as a basis for the analyses, which forms part of the computational test bed developed and presented in Conway *et al.* [1]. Atherosclerotic tissue is varied from being a homogenous continuum to having a lipid rich core, to also having diffuse calcifications throughout. Several material models are also investigated as the base atherosclerotic tissue matrix in the analyses. This includes applying different elastic models to describe the physiological response and then including damage

models which account for the response of the tissue to supra-physiological loading. Using this artery model within the computational test bed, analysis focuses on the deployment of a generic stent geometry using balloon expansion. The response of the system is assessed in terms of tissue deformation and stress state.

Materials & Methods

Geometry & Meshes

The commercially available Abaqus/Explicit solver (DS SIMULIA, USA) is used for all computational modelling performed in this work. For the analyses, a 50% stenosed three layer arterial model geometry, labelled SAL50, (abbreviated from Straight Artery with Lesion of 50%, illustrated in Figure 1, see also Conway *et al.* [1]) is used. This geometry consists of a 0.5 mm thick non-diseased arterial wall equally divided into three layers representing the intima, media and adventitia. The stenosis is considered semi-ellipsoidal in shape and blocks 50% of the available lumen by area, at the maximum axial cross-section. Each section was meshed with 3D eight noded reduced integration linear continuum hexahedral elements. The final mesh for the SAL50 geometry consists of 130064 elements, arrived at after a sensitivity study with the convergence criterion that the maximum von Mises stresses, at specific spatial locations, converge within 5%. A thin outer layer of four noded linear reduced integration shell elements, is also included in the arterial model to represent the physiological environment in which an artery would be embedded.

To examine the response of inhomogeneous atherosclerotic tissue to stenting, two further modifications are included in the SAL50 model. The first is the inclusion of a lipid pool section as shown in Figure 1 and the second is the inclusion of diffuse calcified particles as shown in Figure 2. The volume of lipid included represents 9.3% of the total atherosclerotic tissue volume. The calcified particles are randomly distributed in the atherosclerotic bulk;

630 calcified particles are used, representing 0.5% of the total atherosclerotic tissue volume and the volume of a single particle is approximately 0.0002 mm³, determined from observation of histological sections of diseased tissue in Stary[39]. To allow assignment of the calcified regions the element size had to be reduced to represent an individual calcified particle, resulting in a mesh size increase to 726958 elements. The resulting mesh density was deemed acceptable while still allowing solutions to be generated in a reasonable time frame; typical simulation times are quoted in below in the Analysis of Results section.

A generic stent geometry is used in this study that is representative of the Cypher closed-cell stent, as used previously in Conway *et al.*[1]. The mesh generated consists of 30000 eight noded reduced integration linear continuum hexahedral elements. This was compared with published mesh densities [40,41] for similar stent designs and was deemed acceptable based on these comparisons. The balloon catheter and guidewire delivery system are based on designs presented in the work of Mortier *et al.* [41]. The guidewire has a diameter of 0.2 mm and the catheter is modelled with a diameter of 0.22 mm. The balloon in its unwrapped configuration reaches a diameter of 3 mm. The wrapping of the balloon is simulated by the method outlined in Laroche *et al.* [42], and explained in Conway *et al.*[1].

Constitutive Models

Each layer of the non-diseased arterial wall is considered incompressible and anisotropic and the model proposed by Gasser *et al.*[43] is applied. This model and the values for the material constants are fully described in Conway *et al.*[1] and for brevity are not repeated here. The thin outer layer of shell elements is considered to be isotropic and to be linear elastic in terms of finite deformation strain and stress measures. It has a Young's Modulus of $E = 50$ kPa and a Poisson's Ratio of $\nu = 0.3$, and has a thickness of 0.1 mm. A similar approach was applied

by Harewood *et al.* [44] so that physiologically representative boundary conditions could be applied to the artery.

For the atherosclerotic tissue several material models are investigated. The first approach utilises the second order polynomial incompressible hyperelastic form published by Pericevic *et al.* [2] (full details given in [1] and not repeated here for brevity) referred to in the present paper as the P2 model. The P2 model is based on the tensile testing response of atherosclerotic tissue carried out by Loree *et al.* [18]. The second approach utilises the data published by Maher *et al.* [23], which resulted from the testing of atherosclerotic tissue in compression. A first order incompressible Ogden model (Ogden N1 – with ‘N’ representing the number of terms in the model) (Ogden model framework detailed in [45], and not repeated here for brevity) was fitted to this compressive test data. The third approach combined the Loree tensile data [18] with the Maher compressive data [23] to fit a sixth order incompressible Ogden model (Ogden N6) describing the response of the tissue in tension and compression (once again, detailed in [45], and not repeated here for brevity). Figure 3 shows the uniaxial responses of the three models in tension and compression. As can be seen from the figure, the behaviour of the Ogden N6 model is significantly stiffer in tension than compression, reflexive of the respective experimental data sets ([46] vs. [47]). This difference in experimental tension vs. compression behaviour has also been noted and discussed in Alyildiz *et al.* [35], where it has been attributed to the presence of collagen fibres in the plaque tissue which participate to a much greater extent in load carrying in tension relative to compression. Having said this however it must also be realised that there is significant variability in reported tissue mechanical properties, as is well acknowledged [33,35,36], making it difficult to definitively generalise on relative tensile and compressive stiffnesses.

The three approaches described only give the response of the tissue to physiological loading. To account for supra-physiological loading due to stent implantation, the elasticity models for

the atherosclerotic tissue are combined with different damage modelling approaches. The P2 model is combined with a perfect plasticity model, as per the approach of Gastaldi *et al.* [3], and as used in Conway *et al.* [1], to limit the stresses supported by the atherosclerotic tissue, and a yield stress of 0.4 MPa is assumed. The compressive data published by Maher *et al.* [23] gave the cyclic response of the tissue to loading. In that paper the authors fitted their own damage model to capture the stress softening and permanent set observed within the tissue during loading. Here, using the cyclic response data [23] the Abaqus Mullins effect model is calibrated to the Maher data and combined with the Ogden N1 model. The Mullins effect model within Abaqus is an implementation of the Ogden and Roxburg [48] discontinuous damage model that is characterised by stress softening of an elastic material upon unloading; for details see references [45,48]. A similar procedure is carried out for the Ogden N6 model. The response of the Ogden models incorporating the Mullins effect to strain controlled cyclic loading is illustrated graphically in Figure 4. The response of the P2 model with perfect plasticity to monotonic loading is also shown.

The calcifications are considered to be isotropic and to be linear elastic in terms of finite deformation strain and stress measures. They have a Young's Modulus of $E = 1$ GPa and a Poisson's Ratio of $\nu = 0.3$. The stiffness of the particles is taken from the experimental data of Ebenstein *et al.* [29]. The lipid pool is considered to be isotropic, to behave as a very soft incompressible solid and is modelled using the isotropic part of the Gasser *et al.* [43] material model, which reduces to a Neo-Hookean representation, with a material constant of 0.05 kPa.

The elastic behaviour of the stent is considered to be linear and isotropic in terms of finite deformation stress and strain measures, with a Young's Modulus of $E = 200$ GPa and Poisson's Ratio of $\nu = 0.28$ (representative of biomedical grade stainless steel alloy 316L). Plasticity is described by isotropic hardening J_2 flow theory, where the specific form of the strain hardening curve is taken from McGarry *et al.* [49], including a yield strength of 264

MPa and an ultimate tensile strength (UTS) of 584 MPa at an engineering plastic strain of 0.247. This methodology is consistent with the general approach taken in the literature for stent deformation, for examples see [50–52].

In the stent deployment assembly, a semi-compliant nylon balloon mounted on a high density polyethylene catheter positioned using a nitinol guidewire is used. Each are modelled as behaving as linear and isotropic in terms of finite deformation stress and strain measures, similar to the approach documented in Mortier *et al.* [41]. The guidewire deformations are assumed to be small and superelastic properties of nitinol are neglected. The values for the elastic constants for each component are given in Table 1, included also is the mass proportional Rayleigh damping coefficient, α , used for each component in the delivery system. For the balloon in particular, this means that unrealistic diameter fluctuations during the inflating and unfolding of the balloon are avoided through energy dissipation.

Boundary Conditions & Loading

To allow application of appropriate boundary conditions to the arterial segments, a 10 mm length of straight three layer arterial mesh is added to both ends of each arterial segment, as described previously in Conway *et al.* [1]. The proximal and distal extremities of the extended arterial model are then constrained in all directions. This is to allow for more representative arterial behaviour during the balloon inflation and deflation. The proximal and distal ends of the layer of shell elements surrounding the arterial vessel are also pinned. The inclusion of this layer of elements adds more stability to the analyses as this material is assigned a mass proportional Rayleigh damping coefficient similar to that used for the balloon-catheter assembly components. A coefficient of friction of 0.2 is applied to all contacting surfaces during deployment analyses, as per the approach of Mortier *et al.* [41]. As described previously in Conway *et al.* [1], the pressure applied to the inner surface of the folded balloon is 1.1 MPa which was determined from a free expansion simulation.

Analysis of Results

The first quantity of interest in the simulations performed is the deformed lumen shape. To examine this, a python script was generated which calculates the lumen cross-sectional area based on the deformed nodal coordinates in the Abaqus output data for a sequence of circumferential paths along the length of the lesion. For each material model investigated the lumen cross-sectional area along the length of the atherosclerotic tissue is plotted. To compare each model macroscopically, an average lumen cross-sectional area is calculated and compared with the reference lumen area. All the above are evaluated at two time points for each model, at maximum balloon inflation and post balloon deflation.

The second quantity of interest is the stress state in the non-diseased arterial wall. The variation of the constitutive behaviour of the atherosclerotic tissue has an effect on the stresses transferred to the non-diseased arterial wall. The percent tissue damage risk (as defined in Conway *et al.* [1]) is calculated in each non-diseased arterial layer for each variation in constitutive model. This value determines the proportion of elements with von Mises stresses exceeding reported UTS values for each arterial layer compared to the total number of elements [1].

Finally, the third quantity of interest is the stress state in the diseased atherosclerotic tissue and for this several sets of stress contour plots were examined at two time points, maximum balloon inflation and post deflation.

Run times for these analyses were on the order of 400 CPU hours each on a SGI Altix ICE 8200EX cluster, and the run time more than doubled when the mesh density was increased to include calcifications in the analyses.

Results

Deformed Lumen Measurements

The first atherosclerotic tissue model to be examined in terms of deformed lumen measurements is the Ogden N1 model. Figure 5 - B, D show the results for the cross-sectional area along the length of the lesion for the Ogden N1 model (OgN1), with and without inclusion of the Mullins effect and the lipid pool. Two time points are examined, maximum balloon inflation and post balloon deflation. Clearly apparent in Figure 5 are the many “jagged” regions along the deformed lumen lines. This is indicative of the general compliance of the lesion material that is allowing localised indentation around the stent struts. The first point to note is that the behaviour at the two time points is different due to vessel recoil, and this is manifested in terms of two distinct “tiers” in Figure 5. The Mullins effect is only formally activated on unloading and in the top tier the curves show that the lumen deformations, with and without Mullins, are in agreement at maximum inflation, within the bounds of numerical accuracy for models of such complexity. Note that the lipid pool has only a minimal effect at maximum inflation.

Even though the Mullins effect is active on unloading, consideration of the bottom tier of results in Figure 5 for deflation shows that inclusion of the Mullins effect has little influence on the response of the Ogden N1 model. On the other hand, the inclusion of a lipid pool does generate a noticeable effect, most significantly in terms of a redistribution of the lesion deformation along the length of the lesion, in particular local to the stent struts, emphasised by the deformed plot states in Figure 7- C, D.

Figure 5 - G shows the results for the inclusion of diffuse calcifications in conjunction with the Ogden N1 (OgN1) model, with and without the Mullins effect. One observes a significant difference when calcifications are included, if Figure 5 – B, D and Figure 5 - G are compared.

The calcifications not only affect the unloaded configuration and the distribution of lesion deformation along the length of the lesion but also the maximum cross-sectional area achieved by the stented lumen. In general the presence of calcifications appears to lower the lumen cross-sectional area.

Figure 5 – A, D show the results for the cross-sectional area along the length of the lesion for the Ogden N6 model (OgN6), with and without inclusion of the Mullins effect and the lipid pool. The results at maximum balloon inflation are very similar, as for the Ogden N1 case. However in contrast to the Ogden N1 case, on unloading the results remain quite similar; again, the inclusion of the Mullins effect produces little difference on the luminal measures, but additionally, this time, the analyses appear to be not that sensitive to the presence of a lipid pool.

The next case to be examined is that for the P2 model for the lesion, again at two time points, inflation and deflation, with and without plasticity and with and without a lipid pool present.

Figure 5 – C, F show the results for lumen cross sectional area along the length of the lesion. To remind the reader, the P2 model is much stiffer in tension and in compression than the Ogden N1 model (as shown in Figure 3) so the lumen deformations are much smoother around the stent struts due to this increase in stiffness. Secondly there is significant difference at maximum balloon inflation between the pure hyperelastic polynomial and hyperelastic in combination with plasticity. There is more lumen gain when the plasticity model is used, as due to its characteristics the stress is limited, which encourages straining within the tissue.

The difference between the respective curves on deflation of the balloon is also significant. The difference between the curves with plasticity is less than the difference between the pure hyperelastic curves. This indicates that vessel recoil is less on inclusion of plasticity (an effect noted in the authors' previous work [1]). Finally, the inclusion of a lipid pool in this set

of analyses tends to increase the lumen gain in the middle region of the lesion in all cases. This is most likely due to a softening effect on its inclusion, relative to the stiffness of the P2 material, which means it is easier to deform the tissue. However, the effect is much less than the effect of plasticity on its own.

Figure 6 shows the results for the percentage difference in the *average* lumen area compared with the reference lumen area, at maximum balloon inflation and post balloon deflation, for all models discussed above. A value of zero on this graph indicates that the overall *average* cross-sectional area is the same as the required reference lumen area, i.e. no net difference between the overall deformed cross-sectional area and the reference lumen area. A positive value on this graph indicates that the average cross-sectional area is greater than the reference lumen area and conversely a negative value indicates that the average lumen cross-sectional area is less than the reference lumen area. From Figure 6 it can be observed that this quantity, due to its macroscopic nature, is probably the least sensitive to model changes of the measures considered here. At maximum balloon inflation the percent change varies only between 7 to 11 percent for all material models. Differences post balloon deflation are more significant, where the percent change varies between -5 to 4.5 percent for all material models. Differences are negative, i.e. less than the reference lumen area (least lumen gain), when calcifications are included and when the polynomial model is used. Also to note in the case of negative differences, is that the stent expanded the vessel relative to the diseased state but did not reach the unstenosed vessel area. In these cases the stent design is being more challenged in its scaffolding ability due to the stiffness of the lesion material. From Figure 6 the inclusion of calcifications does have a noticeable overall effect of stiffening the lesion material, while inclusion of plasticity has a substantial softening effect on the P2 response; the effect of the lipid pool is much less significant, for all of the base elasticity models used.

Overall, the results shown in Figure 5 and Figure 6, suggest that the stiffness of the base elasticity model may be the most important parameter in determining the luminal measures considered here. The lipid pool does appear to have an effect locally in the lesion, which is dependent on the base elasticity model, but not significantly in terms of the overall average behaviour. The calcifications and the plasticity each have noticeable effects, both locally and on average. However, the inclusion of the Mullins effect does not appear to be that important, at least for the range of base elasticity models for the lesion considered here.

Tissue Damage Risk

Next the stress state in the non-diseased arterial wall at two time points, maximum balloon inflation and post balloon deflation is examined. Table 2 shows the predicted percent tissue damage risk results in each arterial layer, for all atherosclerotic tissue models previously discussed, in the SAL50 model, with a homogenous lesion representation and with a lesion with a lipid pool and with a lesion with calcifications.

In the first case, of a homogenous lesion, as expected, the predominant percent tissue damage risk occurs in the innermost layer, the intima, with substantially less damage likely in the outer two layers. The stiffer lesion as represented by the P2 model seems to inflict the greatest damage in all three layers. The least stiff model, Ogden N1, results in less damage to the intimal layer and negligible damage to the other two layers by comparison. In all cases, the results indicate that damage is greater at maximum balloon inflation, as would be expected. For this particular performance measure, the Mullins effect has only a very minor influence. Relative to this the inclusion of plasticity with the P2 model has a somewhat greater influence, in particular for the medial and adventitia layers.

The effect of including a lipid pool is shown in the percent tissue damage risk results in the second case of Table 2 for all six types of atherosclerotic lesion modelled. A very similar

trend can be observed when compared with the previous case but on the whole the percent tissue damage risk is slightly less in all cases. This suggests an overall slight softening effect due to the presence of the lipid pool, which is consistent with the general trend observed for the luminal cross-sectional area results.

Finally, the effects of including calcifications in the base atherosclerotic matrix, on the percent tissue damage risk are compared in the third case of Table 2. The base atherosclerotic matrix is modelled using the Ogden N1 model and results are shown with and without the Mullins effect. The inclusion of a small percentage of calcifications results in stiffening and an increase in percent tissue damage risk, and this even becomes apparent in the medial layer.

Stress Distribution in Atherosclerotic Tissue

The reader is referred to Figure 7 for examples of the stress state in the deformed atherosclerotic tissue modelled with Ogden N1, at maximum balloon inflation and post balloon deflation, with and without the lipid pool and calcifications. The first point to note is the overall differences in stress level between the respective plots in the two columns in

At maximum balloon inflation (left column – Figure 7- A,C,E) the atherosclerotic tissue is more highly stressed than after balloon deflation (right column –Figure 7 - B,D,F). This is to be expected as after the balloon is deflated it is only the stent that is exerting a load on the artery, as the vessel attempts to return to its original stress state. The inclusion of a lipid pool lowers the overall stress in the atherosclerotic tissue whereas the inclusion of calcified particles increases the overall stress in the tissue. Interestingly, when calcifications are present the von Mises stress in the non-calcified tissue is increased around the stent struts.

The von Mises stress is, however, is a positive scalar quantity that gives a good indication of the multi-axial stress state magnitude but does not capture whether the material is in tension or compression. For this reason, the maximum and minimum principal stresses at maximum

balloon inflation are also examined. In Figure 8 the minimum and maximum principal stresses in atherosclerotic tissue modelled with Ogden N1, with and without the lipid pool and calcifications are shown. From the minimum principal stress plots (left column Figure 8 - A,C,E) and the maximum principal stress plots (right column Figure 8-B,D,F) the most widespread stress levels (i.e. covering the greatest luminal area) in the lesion are determined and summarised in Table 3, in addition to the peak maximum principal stresses. This analysis is repeated for the other two elasticity models and the relevant values are also summarised in Table 3. Interestingly the compressive stresses appear dominant in the soft Ogden N1 model whereas in the stiffer P2 model the tensile stress appear more dominant. This highlights again the importance of appropriate mechanical characterisation of plaque tissue and its representation *in silico*.

Discussion

The main focus of this paper is to gain insight into the level of detail that is necessary and appropriate when modelling the response of atherosclerotic plaque tissue to stenting, and then to use these results to generate recommendations for the FDA for their guideline document for non-clinical engineering tests for coronary stents[38].

The most significant conclusion to emerge from a detailed examination of the deformed lumen is that the choice of base atherosclerotic elasticity model is the overriding factor controlling lumen deformation. Secondly, the inclusion of the Mullins effect does not have significant effect on the deformed shape, whereas the inclusion of plasticity, as found in Conway *et al.*[1], does have a significant effect on the results for deformed lumen measurements. The inclusion of the Mullins effect does not limit the stress the tissue can support on loading, in contrast to perfect plasticity, which means that straining is encouraged when plasticity becomes active and this then affects the deformed lumen shape and size (Figure 5 and Figure 6).

Looking at the results locally, i.e. the deformations around the stent struts, one can see that the inclusion of a lipid pool with surrounding matrix of tissue modelled with Ogden N1 induces a redistribution of lesion deformation along its length, and in particular generates a lower cross-sectional area around the struts post balloon deflation; on deflation, the lipid pool. However, when the surrounding matrix is modelled with the much stiffer Ogden N6 model the local deformation distribution results are very similar, with and without a lipid pool. This is also the case for the P2 model. This indicates that presence of a lipid pool may only have an effect on a very soft surrounding matrix and less so on a stiff surrounding tissue.

Looking at the inclusion of calcifications surrounded by a tissue matrix represented by the Ogden N1 model, a high variability in computed lumen deformation results is evident. The presence of the calcifications affects the local deformation both at inflation and on deflation. For the same given applied pressure to the balloon expanding the stent, the same deformed lumen is not achieved when calcifications are present. On deflation, the inclusion of 0.5% calcifications, by volume, reduces the range in lumen cross-sectional area by 0.2 mm^2 or 3%. This implies that for even a small volume of calcifications present in a lesion (in this case 0.5% of the total lesion volume) the cardiologist may have to inflate to a higher pressure to gain the desired lumen cross-sectional area. This is evident clinically also, as when calcifications are present sometimes a subsequent balloon inflation (with pressures up to 20 atm) has been reported if adequate stent expansion is not achieved [53]. From a macroscopic perspective, the current study shows that stent expansion for a given balloon pressure is reduced when calcifications are present. The higher stiffness of plaque tissue when calcifications are present, as noted here, is consistent with experimental tissue testing observations [16,34].

From a percent tissue damage risk perspective for the non-diseased outer arterial layers, the inclusion of the Mullins effect on the base atherosclerotic tissue behaviour does not have a

significant effect, whereas the inclusion of plasticity has a relatively more significant effect. As a step toward representation of supra-physiological loading response the inclusion of plasticity could be recommended. As the inclusion of plasticity in the atherosclerotic tissue limits the stress supported by the tissue, it encourages redistribution of the stress in the non-diseased arterial wall thus resulting in higher (and hence more conservative) predicted tissue damage risk. The results for the presence of a lipid pool indicate a somewhat softer overall atherosclerotic body in the simulations. Whereas the presence of diffuse calcifications increases the percent tissue damage risk in the Ogden N1 case modelled by 7%, which is consistent with calcifications increasing the plaque stiffness as noted above.

In relation to the micromechanical stress state in the lesion itself, as summarised in Table 3, and focusing on the results for the most widespread minimum and maximum principal stresses, it can be seen for the (relatively soft) Ogden N1 material that the compressive minimum principal stress range is an order of magnitude greater than the tensile maximum principal stress range (0 – 1.9 MPa vs. 0 – 0.12 MPa), indicating a predominant (radial) compressive mode of loading. However, in contrast, for the significantly stiffer P2 material, the maximum tensile principal stress range is almost three times larger than the minimum compressive principal stress range (0 – 1.27 MPa vs. 0 – 0.5 MPa), indicating a predominant (circumferential) tensile mode of loading. This illustrates the importance of mechanically characterising atherosclerotic tissue in both tension *and* compression to fully capture the tissue behaviour, as this has important implications for the *in silico* deformation and stress state of the tissue during loading. These computed data allow for an assessment of plaque rupture risk. The availability of plaque mechanical properties, and in particular rupture properties, as discussed above, is limited; however a plaque rupture stress threshold of 300 kPa, originally due to Cheng *et al.* [54], is widely quoted [14,16,33]. Cheng *et al.* [54] also reported an average rupture stress of 545 kPa \pm 160 kPa. From a consideration of the

published data to date, as recently reviewed [14,16,33,55], we believe that these values are quite reasonable for the purpose of making a basic assessment of the current model predictions. The stresses quoted above are Peak Circumferential Stresses (PCS), a measure that is commonly quoted in the literature when considering vulnerable plaque caps in particular [16,56]; this is a normal stress and in the context of the present model is arguably best compared with the predicted maximum principal stress [14]. Using the 300 kPa threshold, it is clear from Table 3 that for all but the first two cases with the softest base elasticity (OgN1, OgN1+lipid), the models predict that the expansion of this particular stent design could generate a plaque rupture risk.

In addition to a principal stress-based assessment of plaque rupture risk, a limited von Mises stress based assessment is also possible, but based on even more limited rupture data. Using finite element models derived from MRI imaging of vulnerable plaques, Li *et al.*³³ reported a von Mises stress of 683.3 kPa for vulnerable plaques that had ruptured and a von Mises stress of 226.9 kPa for those that had not ruptured. Applying a critical von Mises stress of 683.3 kPa to the present simulation results leads to essentially the same plaque rupture risk conclusions, as indicated for example by the extensive areas of high von Mises stress around the stent struts for the Ogden N1 with calcifications case relative to the Ogden N1 and Ogden N1 with lipid pool cases. Extensive areas of high von Mises stress (>683.3 kPa) are also observed for the remaining four cases considered above: OgN6, OgN6+lipid, P2, P2+lipid (results not shown).

Consistent with the previous observations, the model predictions, in this case for the plaque rupture risk, are clearly strongly dependent on the choice of base atherosclerotic elasticity model, and also the choice of threshold stress, with the stiffer models indicating higher risk based on a single threshold stress, developing on the work of Timmins *et al.* [8] who carried out finite element analyses of stent deployment in the presence of plaques of varying

stiffness. Deformed radial position values were also plotted similar to the approach taken in Figure 5 presented in this work and the comparative qualitative behaviour is in agreement, in that the stiffer the base elasticity model, of the atherosclerotic tissue, the less expansion is observed.

The strong influence of the calcified particles in increasing rupture risk is also clearly evident, as shown for the Ogden N1 case considered in this work. The calcifications clearly induce local stress concentrations in the plaque at the lumen surface. This is consistent with the computational modelling work of Maldonado *et al.* [56] and others [58–61], that has been focused on stress analysis of micro-calcifications in vulnerable plaque caps, and that indicate stress concentrations of up to 5 [56], or up to 16 [61] in the cap tissue local to clustered micro-calcifications. In relation to reported plaque rupture properties more generally, experimentally determined rupture properties are strongly tissue type specific, as recently reviewed as discussed above [16,17]; for example an average lipid dominant plaque rupture stress of 342 kPa and a calcified plaque rupture stress of 618 kPa are reported in [34].

The strong model sensitivities evident from the discussion this far clearly point towards the need for more detailed testing to generate accurate atherosclerotic tissue component-specific mechanical properties for both (i) constitutive behaviour to high strain and (ii) rupture, reflexive of supra-physiological loading experienced in stenting. Further, they substantiate the statements in Holzapfel *et al.* [14] on the need to identify and develop better failure criteria for plaque components, and the associated need for more experimental, analytical and numerical studies of plaque components [17]. The strong model sensitivities shown here also help address the question posed in Gijsen and Migliavacca [17] on whether multiscale plaque features need to be included in models for stress and strength analyses; our analyses suggest that multiscale plaque features should be included for accurate stress analyses. This is critically important in the further development of models for the test-bed, so that the lesion

rupture risk of different stent designs can be accurately assessed as part of the stent design process.

Also to be considered are the limitations of this work. The assumption that the atherosclerotic tissue is isotropic, when in reality it is probably anisotropic due to the presence of collagen fibres, is a limitation. Another assumption, with regard to soft tissue, is material rate independence, although these tissues are most likely rate dependent and viscoelastic. Again, adequate experimental data for this behaviour is currently lacking. A third assumption is with regard to the representation of the lipid pool as a soft solid when it may be more appropriate to model it as a viscous fluid. A further limitation is the morphology of the microcalcifications presented which are approximated as “brick-like” and dependent on element shape. The distribution of microcalcifications could also be increased and the particles allowed to coalesce as per a more advanced representation of the disease [62]. This could be developed for future applications of the test-bed approach presented here. Also not considered was axial pre-stretch or residual stress within the vessel wall or the explicit representation of cardiac wall and surrounding tissues. The pressure due to pulsatile blood flow was not modelled as it was deemed that it was insignificant with respect to the force exerted by the stent implantation. However with regards the pressure change due to blood flow this may affect the damage accumulating due to stent implantation. This plaque damage modelling would require the use of more sophisticated and/or micromechanically based continuum damage approach – but such an in-depth focus was considered to be outside the scope of the present study.

A final point on the approach taken in this work is that, similar to previous work [1], it is “population specific” and may create a working database or library to inform device designers as regards the range of patient responses to device implantation. This can complement the work performed in the patient specific modelling space also.

Conclusions and Recommendations

Overviewing the results of the investigations (in terms of deformed lumen areas, predicted tissue damage risk and lesion microscale stress state) one is led to the central conclusion that, for stenting applications, the base elasticity model for the atherosclerotic tissue is the key aspect of the lesion modelling (for a given stenosis level) that determines the overall computational test-bed predictions; the choice of elasticity model dominates over the representation of plaque constituents and the inclusion of lesion tissue damage modelling (Mullins effect, plasticity).

Having said this though, the plaque constituents and damage models are important, but to varying extents. As regards plaque constituents, the effects of calcifications are more significant than those of the lipid pool; even a small volume fraction of the former generates noticeable increases in lesion stiffness and stress levels, whereas a relatively large lipid pool induces only a modest softening overall with significant effects being observed only in the very soft base elasticity case (Ogden N1) at the level of local lesion deformation around the stent struts. As regards the lesion tissue damage modelling, plasticity is substantially more influential than the Mullins effect, in terms of inducing overall softening and stress redistribution in the tissue; in the context of the simulations considered here, the Mullins effect is not of primary importance. This may prove to be a useful result in guiding the identification and development of future failure criteria[14] and damage models for plaque components.

In relation to the base elasticity of the atherosclerotic tissue, both the tensile *and* compressive behaviour are of critical importance. Additionally, an accurate knowledge of local lesion local rupture stress and strain would also guide the development of improved failure criteria [14]. This highlights the need for further careful mechanical characterisation of lesion tissue in terms of multi-mode mechanical testing up to rupture and the quantification of the local

rupture strain and stress state. In this context the test standard for uniaxial tensile testing of atherosclerotic tissue proposed in [33] is a useful development. However, given the complex deformation of plaque during stent deployment, the current study provides strong motivation for multi-axial mechanical testing, including biaxial and confined compression tests. Following the experimental approach used by Kelly and McGarry[63] for cancellous bone, confined compression should be performed in parallel with uniaxial tests to determine if plaque undergoes pressure dependent yielding. Based on previous finite element simulations using a crushable foam plasticity model it could be expected that the occurrence of pressure dependent yielding would further reduce the load bearing limit of the plaque, further increasing the stress in the arterial tissue during angioplasty [64].

The current FDA guidelines for non-clinical engineering tests do not explicitly require the modelling of a lesion in their stress-strain analysis section in relation to stent deployment modelling. In Conway *et al.* [1], it was strongly recommended that for assessing device performance the presence of a lesion should be accounted for in computational models, and also that the quantity of lesion tissue should be varied. Building on these recommendations, from the results of this study the following is also recommended for stent deployment modelling in a virtual stenotic vessel:

- The elastic behaviour of the atherosclerotic tissue represented in the models should cover a range of response types (stiff to compliant) due to the significant variation in experimentally determined tissue properties reported in the literature.
- A comparison local (microscale) stress and strain with the local rupture state (rupture stress and strain) of the atherosclerotic tissue should be included in the modelling for meaningful device performance assessments to be made. This comparison should be tissue type specific (lipid plaque, calcified, etc.), due to the strong dependence of the local rupture state on atherosclerotic tissue type.

- Plaque constituents should be considered in atherosclerotic tissue models, such as calcifications and lipid regions, since in both cases their presence will influence the choice of atherosclerotic tissue rupture state for device performance assessment.
- The incorporation of plasticity should be considered for the representation of atherosclerotic tissue damage in the models (due in part to its ease of implementation), in particular when assessing the effects of supra-physiological loading.

Acknowledgements

The authors would like to acknowledge funding from the Irish Research Council/Irish Research Council for Science, Engineering and Technology under the Embark Initiative (C. Conway) and the SFI/HEA Irish Centre for High End Computing for the provision of computational facilities and support.

References

1. Conway C, Sharif F, McGarry J, McHugh P: A Computational Test-Bed to Assess Coronary Stent Implantation Mechanics Using a Population-Specific Approach. *Cardiovascular Engineering and Technology* 2012;3:1–14.
2. Pericevic I, Lally C, Toner D, Kelly DJ: The influence of plaque composition on underlying arterial wall stress during stent expansion: The case for lesion-specific stents. *Medical Engineering & Physics* 2009;31:428–433.
3. Gastaldi D, Morlacchi S, Nichetti R, Capelli C, Dubini G, Petrini L, et al.: Modelling of the provisional side-branch stenting approach for the treatment of atherosclerotic coronary bifurcations: effects of stent positioning. *Biomechanics and Modeling in Mechanobiology* 2010;9:551–561.
4. Zahedmanesh H, John Kelly D, Lally C: Simulation of a balloon expandable stent in a realistic coronary artery--Determination of the optimum modelling strategy. *Journal of Biomechanics* 2010;43:2126–2132.
5. Grogan JA, Leen SB, McHugh PE: Optimizing the design of a bioabsorbable metal stent using computer simulation methods. *Biomaterials* 2013;34:8049–8060.
6. Grogan JA, O'Brien BJ, Leen SB, McHugh PE: A corrosion model for bioabsorbable metallic stents. *Acta biomaterialia* 2011;7:3523–3533.
7. Morlacchi S, Colleoni SG, Cárdenes R, Chiastra C, Diez JL, Larrabide I, et al.: Patient-specific simulations of stenting procedures in coronary bifurcations: two clinical cases. *Medical engineering & physics* 2013 Sep;35:1272–81.
8. Timmins LH, Meyer CA, Moreno MR, Moore Jr. JE: Effects of stent design and atherosclerotic plaque composition on arterial wall biomechanics. *Journal of Endovascular Therapy* 2008;15:643–654.
9. Morlacchi S, Migliavacca F: Modeling stented coronary arteries: where we are, where to go. *Annals of biomedical engineering* 2013 Jul;41:1428–44.
10. Iannaccone F, Debusschere N, De Bock S, De Beule M, Van Loo D, Vermassen F, et al.: The influence of vascular anatomy on carotid artery stenting: a parametric study for damage assessment. *Journal of biomechanics* 2014 Mar 3;47:890–8.
11. Holzapfel GA, Stadler M, Gasser TC: Changes in the mechanical environment of stenotic arteries during interaction with stents: Computational assessment of parametric stent designs. *Journal of Biomechanical Engineering* 2005;127:166–180.
12. García A, Peña E, Martínez MA: Influence of geometrical parameters on radial force during self-expanding stent deployment. Application for a variable radial stiffness stent. *J Mech Behav Biomed Mater* 2012 Jun;10:166–175.
13. Morlacchi S, Pennati G, Petrini L, Dubini G, Migliavacca F: Influence of plaque calcifications on coronary stent fracture: a numerical fatigue life analysis including cardiac wall movement. *Journal of biomechanics* 2014 Mar 3;47:899–907.

14. Holzapfel G a, Mulvihill JJ, Cunnane EM, Walsh MT: Computational approaches for analyzing the mechanics of atherosclerotic plaques: A review. *Journal of biomechanics* 2014 Mar 3;47:859–69.
15. Brinkhues S, Balzani D, Holzapfel GA: Simulation of Damage Hysteresis in Soft Biological Tissues. *PAMM* 2009;9:155–156.
16. Cardoso L, Weinbaum S: Changing views of the biomechanics of vulnerable plaque rupture: a review. *Annals of biomedical engineering* 2014 Feb;42:415–31.
17. Gijsen FJH, Migliavacca F: Plaque mechanics. *Journal of biomechanics* 2014 Mar 3;47:763–4.
18. Loree HM, Grodzinsky AJ, Park SY, Gibson LJ, Lee RT: Static circumferential tangential modulus of human atherosclerotic tissue. *Journal of Biomechanics* 1994;27:195–204.
19. Topoleski LDT, Salunke NV, Humphrey JD, Mergner WJ: Composition- and history-dependent radial compressive behavior of human atherosclerotic plaque. *Journal of Biomedical Materials Research* 1997;35:117–127.
20. Salunke NV, Topoleski LDT, Humphrey JD, Mergner WJ: Compressive stress-relaxation of human atherosclerotic plaque. *Journal of Biomedical Materials Research* 2001;55:236–241.
21. Maher E, Creane A, Sultan S, Hynes N, Lally C, Kelly DJ: Tensile and compressive properties of fresh human carotid atherosclerotic plaques. *Journal of Biomechanics* 2009 Dec 11;42:2760–2767.
22. Lawlor MG, O'Donnell MR, O'Connell BM, Walsh MT: Experimental determination of circumferential properties of fresh carotid artery plaques. *Journal of Biomechanics* 2011 Jun 3;44:1709–1715.
23. Maher E, Creane A, Sultan S, Hynes N, Lally C, Kelly DJ: Inelasticity of Human Carotid Atherosclerotic Plaque. *Annals of Biomedical Engineering* 2011 May 27;39:2445–2455.
24. Walraevens J, Willaert B, De Win G, Ranftl A, De Schutter J, Sloten J Vander: Correlation between compression, tensile and tearing tests on healthy and calcified aortic tissues. *Medical engineering & physics* 2008 Nov;30:1098–104.
25. Teng Z, Tang D, Zheng J, Woodard PK, Hoffman AH: An experimental study on the ultimate strength of the adventitia and media of human atherosclerotic carotid arteries in circumferential and axial directions. *Journal of biomechanics* 2009 Nov 13;42:2535–9.
26. Holzapfel GA, Sommer G, Regitnig P: Anisotropic mechanical properties of tissue components in human atherosclerotic plaques. *Journal of Biomechanical Engineering* 2004;126:657–665.
27. Lee R, Grodzinsky A, Frank E, Kamm R, Schoen F: Structure-dependent dynamic mechanical behavior of fibrous caps from human atherosclerotic plaques. *Circulation* 1991;83:1764–1770.

28. Loree HM, Tobias BJ, Gibson LJ, Kamm RD, Small DM, Lee RT: Mechanical properties of model atherosclerotic lesion lipid pools. *Arteriosclerosis, Thrombosis, and Vascular Biology* 1994 Feb 1;14:230–234.
29. Ebenstein DM, Coughlin D, Chapman J, Li C, Pruitt LA: Nanomechanical properties of calcification, fibrous tissue, and hematoma from atherosclerotic plaques. *Journal of Biomedical Materials Research Part A* 2009 Dec 15;91A:1028–1037.
30. Barrett SRH, Sutcliffe MPF, Howarth S, Li Z, Gillard JH: Experimental measurement of the mechanical properties of carotid atherothrombotic plaque fibrous cap. *Journal of Biomechanics* 2009;42:1650–1655.
31. Chai C-K, Akyildiz AC, Speelman L, Gijsen FJH, Oomens CWJ, van Sambeek MRHM, et al.: Local axial compressive mechanical properties of human carotid atherosclerotic plaques-characterisation by indentation test and inverse finite element analysis. *Journal of biomechanics* 2013 Jun 21;46:1759–66.
32. Barrett SRH, Sutcliffe MPF, Howarth S, Li Z, Gillard JH: Experimental measurement of the mechanical properties of carotid atherothrombotic plaque fibrous cap. *Journal of Biomechanics* 2009;42:1650–1655.
33. Walsh MT, Cunnane EM, Mulvihill JJ, Akyildiz a C, Gijsen FJH, Holzapfel G a: Uniaxial tensile testing approaches for characterisation of atherosclerotic plaques. *Journal of biomechanics* 2014 Mar 3;47:793–804.
34. Mulvihill JJ, Cunnane EM, McHugh SM, Kavanagh EG, Walsh SR, Walsh MT: Mechanical, biological and structural characterization of in vitro ruptured human carotid plaque tissue. *Acta biomaterialia* 2013 Nov;9:9027–35.
35. Akyildiz AC, Speelman L, Gijsen FJH: Mechanical properties of human atherosclerotic intima tissue. *Journal of biomechanics* 2014 Mar 3;47:773–83.
36. Chai C-K, Speelman L, Oomens CWJ, Baaijens FPT: Compressive mechanical properties of atherosclerotic plaques--indentation test to characterise the local anisotropic behaviour. *Journal of biomechanics* 2014 Mar 3;47:784–92.
37. Kolandaivelu K, Leiden BB, Edelman ER: Predicting response to endovascular therapies: dissecting the roles of local lesion complexity, systemic comorbidity, and clinical uncertainty. *Journal of biomechanics* 2014 Mar 3;47:908–21.
38. FDA: Non-Clinical Engineering Tests and Recommended Labeling for Intravascular Stents and Associated Delivery Systems [Internet] [cited 2012 Jun 25];Available from: <http://www.fda.gov/medicaldevices/deviceregulationandguidance/guidancedocuments/u cm071863.htm>
39. Stary H: *Atlas of Atherosclerosis Progression and Regression*. New York/London, Parthenon Publishing, 1999.
40. Mortier P, Beule MD, Carlier SG, Impe RV, Verhegge B, Verdonck P: Numerical Study of the Uniformity of Balloon-Expandable Stent Deployment. *Journal of Biomechanical Engineering* 2008;130:021018.

41. Mortier P, Holzapfel GA, De Beule M, Van Loo D, Taeymans Y, Segers P, et al.: A novel simulation strategy for stent insertion and deployment in curved coronary bifurcations: Comparison of three drug-eluting stents. *Annals of Biomedical Engineering* 2010;38:88–99.
42. Laroche D, Delorme S, Anderson T, DiRaddo R: Computer Prediction of Friction in Balloon Angioplasty and Stent Implantation. *Biomedical Simulation* 2006;4072:1–8.
43. Gasser TC, Ogden RW, Holzapfel GA: Hyperelastic modelling of arterial layers with distributed collagen fibre orientations. *Journal of The Royal Society Interface* 2006;3:15–35.
44. Harewood F, Grogan J, McHugh P: A multiscale approach to failure assessment in deployment for cardiovascular stents. *Journal of Multiscale Modeling* 2010;2:1–22.
45. Anon.: Abaqus 6.10 Theory Manual, DS SIMULIA Corp., Providence, RI, USA 2010;
46. Loree HM, Grodzinsky AJ, Park SY, Gibson LJ, Lee RT: Static circumferential tangential modulus of human atherosclerotic tissue. *Journal of Biomechanics* 1994;27:195–204.
47. Maher E, Creane A, Sultan S, Hynes N, Lally C, Kelly DJ: Inelasticity of Human Carotid Atherosclerotic Plaque. *Annals of Biomedical Engineering* 2011 May;39:2445–2455.
48. Ogden RW, Roxburgh DG: A pseudo-elastic model for the Mullins effect in filled rubber. *Proceedings of the Royal Society of London A* 1999;455:2861–2877.
49. McGarry JP, O'Donnell BP, McHugh PE, O'Cearbhail E, McMeeking RM: Computational Examination of the Effect of Material Inhomogeneity on the Necking of Stent Struts Under Tensile Loading. *Journal of Applied Mechanics* 2007;74:978–989.
50. Chua SND, Mac Donald BJ, Hashmi MSJ: Finite-element simulation of stent expansion. *Journal of Materials Processing Technology* 2002 Jan 15;120:335–340.
51. Bedoya J, Meyer CA, Timmins LH, Moreno MR, Moore Jr. JE: Effects of stent design parameters on normal artery wall mechanics. *Journal of Biomechanical Engineering* 2006;128:757–765.
52. Capelli C, Gervaso F, Petrini L, Dubini G, Migliavacca F: Assessment of tissue prolapse after balloon-expandable stenting: Influence of stent cell geometry. *Medical Engineering & Physics* 2009;31:441–447.
53. Vavuranakis M, Toutouzas K, Stefanidis C, Chrisohou C, Markou D, Toutouzas P: Stent deployment in calcified lesions: Can we overcome calcific restraint with high-pressure balloon inflations? *Catheterization and Cardiovascular Interventions* 2001;52:164–172.
54. Cheng GC, Loree HM, Kamm RD, Fishbein MC, Lee RT: Distribution of circumferential stress in ruptured and stable atherosclerotic lesions. A structural analysis with histopathological correlation. *Circulation* 1993;87:1179–1187.

55. Mulvihill JJ, Walsh MT: On the mechanical behaviour of carotid artery plaques: the influence of curve-fitting experimental data on numerical model results. *Biomechanics and modeling in mechanobiology* 2013 Oct;12:975–85.
56. Maldonado N, Kelly-Arnold A, Vengrenyuk Y, Laudier D, Fallon JT, Virmani R, et al.: A mechanistic analysis of the role of microcalcifications in atherosclerotic plaque stability: potential implications for plaque rupture. *American journal of physiology Heart and circulatory physiology* 2012 Sep 1;303:H619–28.
57. Li Z-Y, Howarth S, Trivedi RA, U-King-Im JM, Graves MJ, Brown A, et al.: Stress analysis of carotid plaque rupture based on in vivo high resolution MRI. *Journal of Biomechanics* 2006;39:2611–2622.
58. Wenk JF: Numerical modeling of stress in stenotic arteries with microcalcifications: A parameter sensitivity study. *Journal of Biomechanical Engineering* 2010;133:014503.
59. Vengrenyuk Y, Carlier S, Xanthos S, Cardoso L, Ganatos P, Virmani R, et al.: A hypothesis for vulnerable plaque rupture due to stress-induced debonding around cellular microcalcifications in thin fibrous caps. *Proceedings of the National Academy of Sciences of the United States of America* 2006 Oct 3;103:14678–83.
60. Rambhia SH, Liang X, Xenos M, Alemu Y, Maldonado N, Kelly a, et al.: Microcalcifications increase coronary vulnerable plaque rupture potential: a patient-based micro-CT fluid-structure interaction study. *Annals of biomedical engineering* 2012 Jul;40:1443–54.
61. Kelly-Arnold A, Maldonado N, Laudier D, Aikawa E, Cardoso L, Weinbaum S: Revised microcalcification hypothesis for fibrous cap rupture in human coronary arteries. *Proceedings of the National Academy of Sciences of the United States of America* 2013 Jun 25;110:10741–6.
62. Stary HC: Natural history of calcium deposits in atherosclerosis progression and regression. *Z Kardiol* 2000 Feb 1;89:S028–S035.
63. Kelly N, McGarry JP: Experimental and numerical characterisation of the elasto-plastic properties of bovine trabecular bone and a trabecular bone analogue. *Journal of the mechanical behavior of biomedical materials* 2012 May;9:184–97.
64. Kelly N, Harrison NM, McDonnell P, McGarry JP: An experimental and computational investigation of the post-yield behaviour of trabecular bone during vertebral device subsidence. *Biomechanics and modeling in mechanobiology* 2013 Aug;12:685–703.

Table 1 Material parameters characterising the elastic constants for the stent deployment assembly.

	E (MPa)	ν (-)	α (-)
Balloon	850	0.4	8000
Catheter	1000	0.4	8000
Guidewire	62000	0.3	8000

Table 2

Values of predicted percent tissue damage risk, as defined in Analysis of Results section, in each arterial layer for the indicated atherosclerotic tissue models and inclusions.

Homogenous Lesion

Model	Intima > 394kPa		Media > 419kPa		Adventitia 1300> kPa	
	Max Inflation	Deflation	Max Inflation	Deflation	Max Inflation	Deflation
P2	73.71	63.08	12.86	3.08	15.13	1.73
P2 + Plasticity	70.26	62.25	6.88	1.67	9.82	1.02
Ogden N1	44.78	34.25	0.81	0.13	0.25	0.06
Ogden N1 + Mullins	43.78	31.29	0.79	0.12	0.23	0.03
Ogden N6	54.17	44.00	1.92	0.63	1.65	0.34
Ogden N6 + Mullins	57.13	44.96	2.05	0.62	1.90	0.32

Lesion with Lipid Pool

Model	Intima > 394kPa		Media > 419kPa		Adventitia 1300> kPa	
	Max Inflation	Deflation	Max Inflation	Deflation	Max Inflation	Deflation
P2	71.53	61.52	11.13	2.79	12.29	1.49
P2 + Plasticity	65.37	55.67	4.93	1.23	6.04	0.62
Ogden N1	39.74	28.17	0.54	0.08	0.21	0.04
Ogden N1 + Mullins	38.32	25.84	0.53	0.11	0.19	0.03
Ogden N6	53.17	42.51	1.51	0.61	1.24	0.28
Ogden N6 + Mullins	53.15	40.59	1.55	0.51	1.30	0.21

Lesion with Calcifications

Model	Intima > 394kPa		Media > 419kPa		Adventitia 1300> kPa	
	Max Inflation	Deflation	Max Inflation	Deflation	Max Inflation	Deflation
Ogden N1 + Calc	41.90	36.45	5.81	4.19	0.00	0.00
Ogden N1 + Mullins + Calc	41.10	35.15	5.75	4.09	0.00	0.00

Table 3 Most widespread maximum and minimum principal stress ranges (i.e. covering the greatest luminal area) in the lesion for different atherosclerotic tissue models at the point of maximum inflation. Peak maximum principal stress also shown.

Model	σ_{\min} range	σ_{\max} range	Peak σ_{\max}
	(MPa)	(MPa)	(MPa)
Ogden N1	0 to -1.9	0 to 0.12	0.189
OgdenN1 + lipid	0 to -1.9	0 to 0.12	0.189
Ogden N1 + calc	0 to -1.9	0 to 0.12	10.0
Ogden N6	0 to -0.47	0 to 0.45	3.4
Ogden N6 + lipid	0 to -0.47	0 to 0.45	3.4
P2	0 to -0.5	0 to 1.27	2.69
P2 + lipid	0 to -0.5	0 to 1.27	2.69

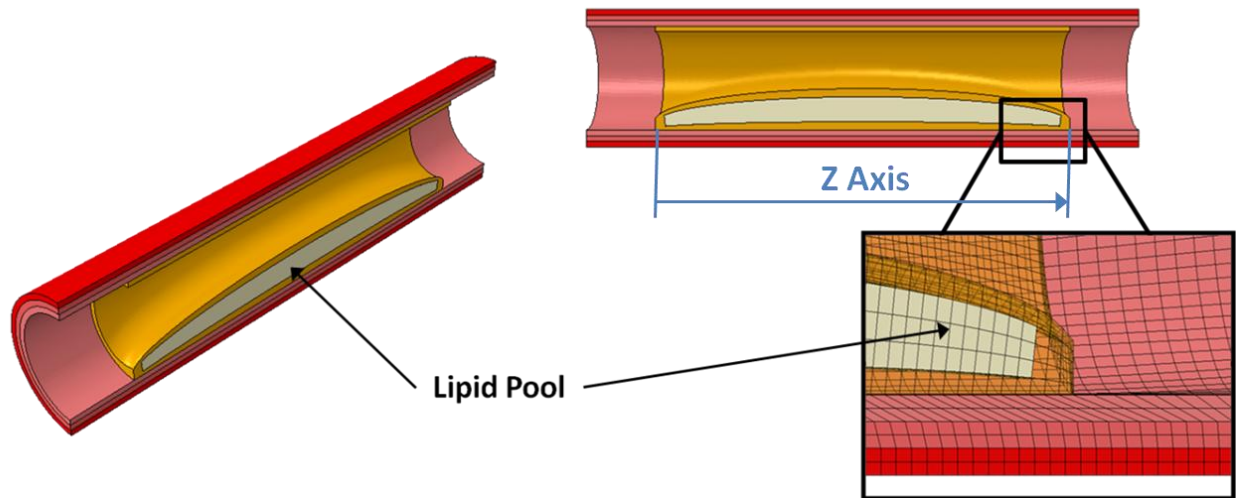


Figure 1 Schematic of lipid pool with SAL50 arterial model, with insert showing mesh density.

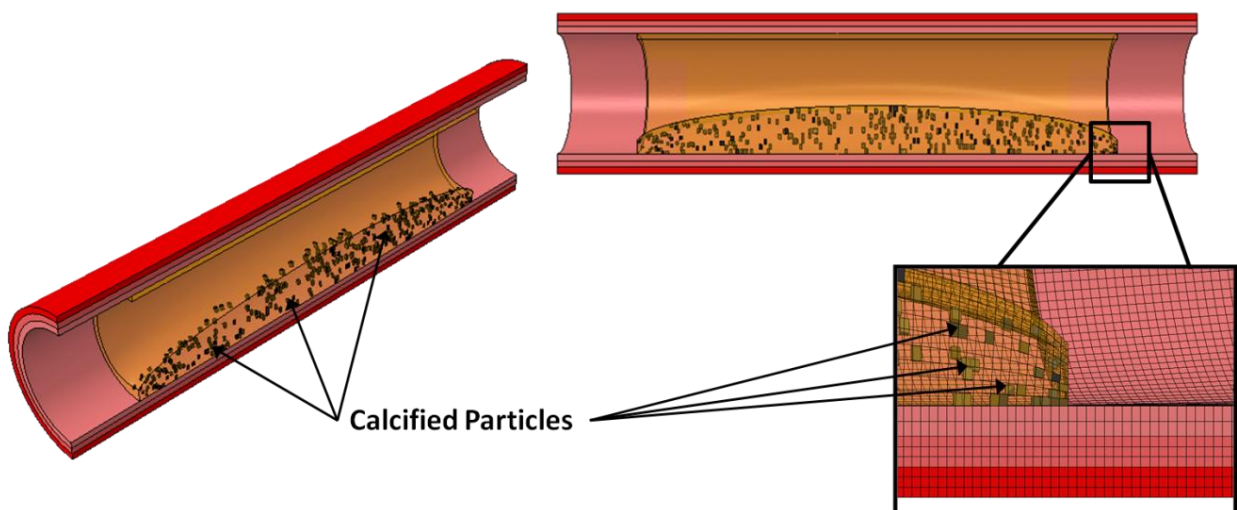


Figure 2 Schematic of calcified regions in SAL50 arterial model, with insert showing mesh density.

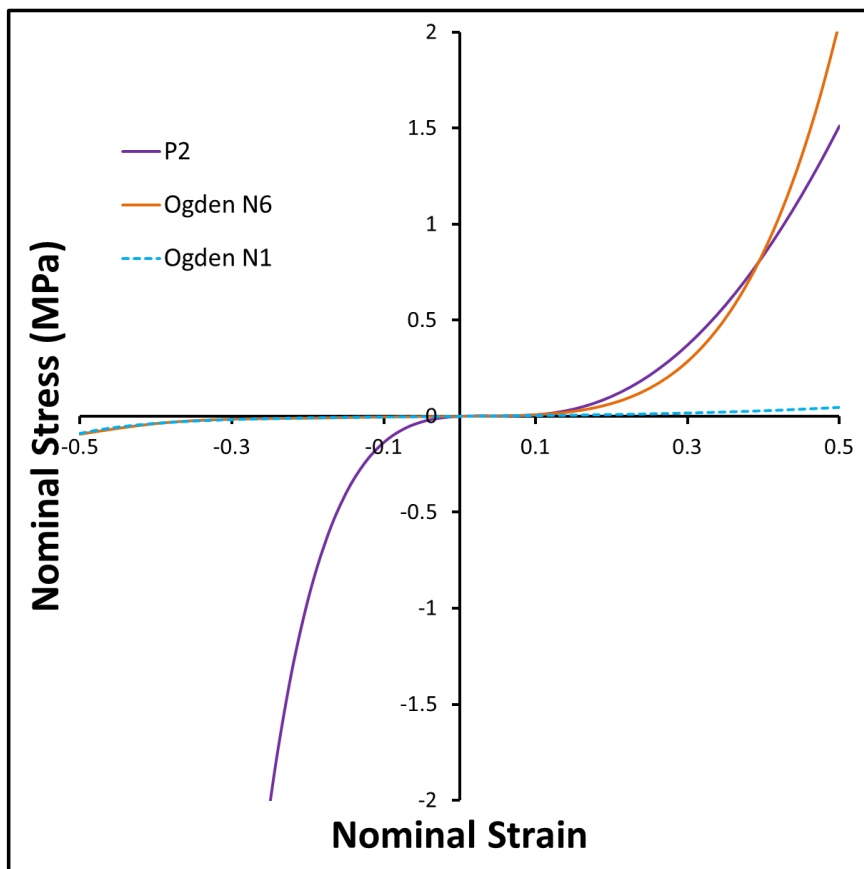


Figure 3 Uniaxial responses of material models for atherosclerotic tissue to monotonic loading in tension and compression.

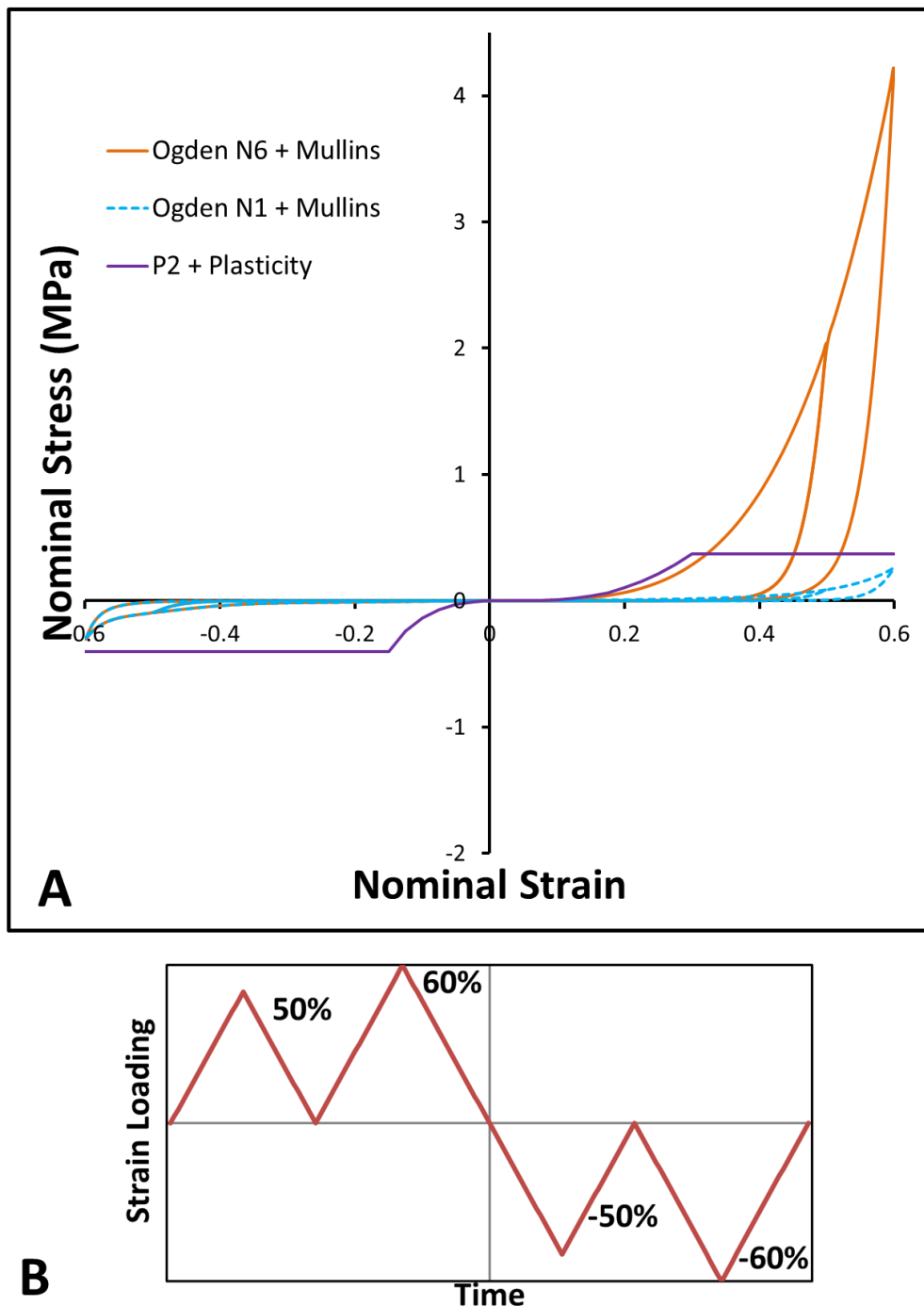


Figure 4 A) Responses of Ogden models, with Mullins effect, to cyclic loading in tension and compression with softening on unloading illustrated. Response of Polynomial model to monotonic loading also shown. B) Cyclic strain loading amplitude.

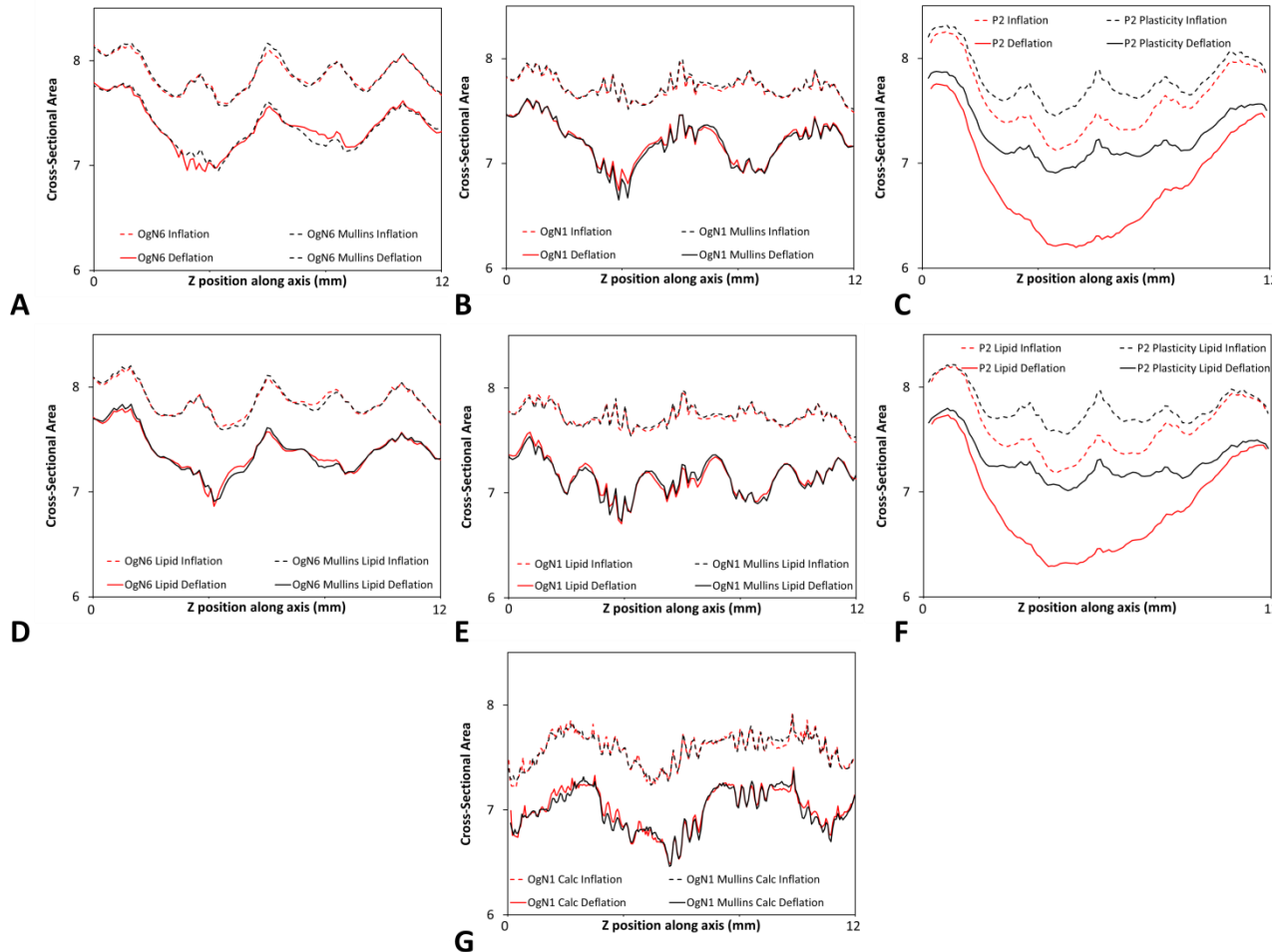


Figure 5 Cross-sectional measurements along the length of the atherosclerotic tissue geometry, Z position along axis (see Figure 1), at inflation and deflation timepoints. A) Ogden N6 with and without Mullins effect, B) Ogden N1 with and without Mullins effect, C) P2 with and without plasticity, D) Ogden N6 with lipid with and without Mullins effect, E) Ogden N1 with lipid with and without Mullins effect, F) P2 with lipid with and without plasticity, G) Ogden N1 with calcifications with and without Mullins effect.

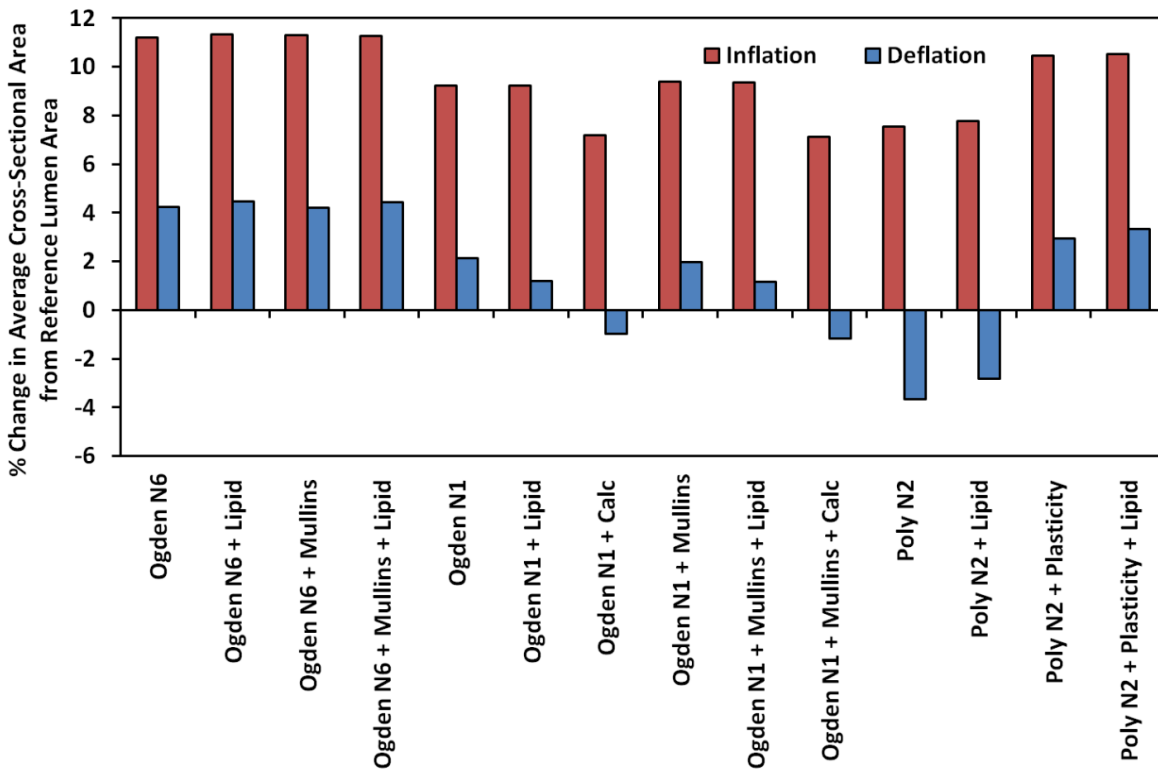


Figure 6 Results for percent change in average lumen cross-sectional area with respect to reference lumen area for all of the atherosclerotic tissue models discussed in text. Data was analysed at two time points, max balloon inflation (red “inflation” series) and post balloon deflation (blue “deflation” series).

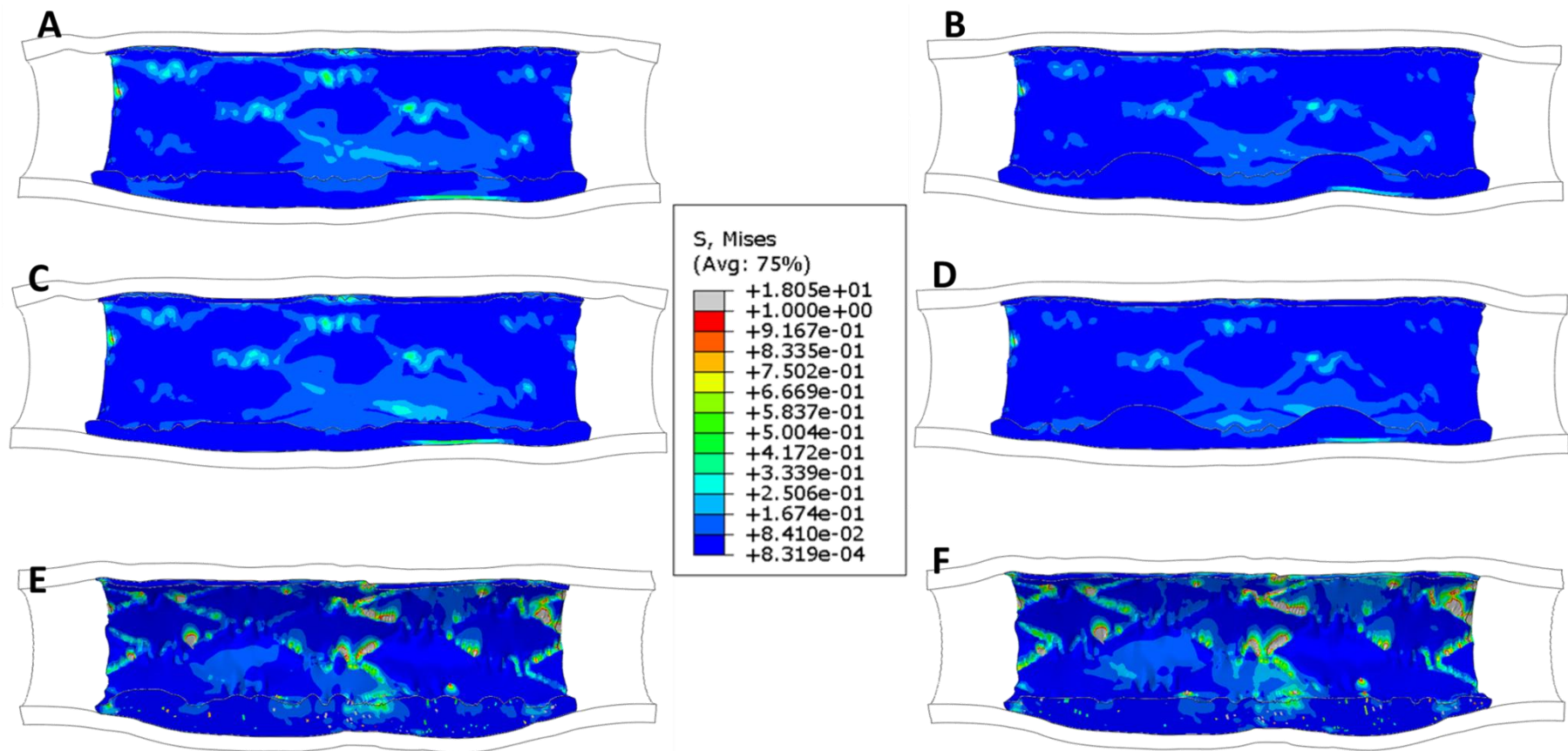


Figure 7 Von Mises stress distribution (MPa) in atherosclerotic tissue, A) Max inflation for Ogden N1 material model, B) Deflation for Ogden N1 material model, C) Max inflation for Ogden N1 material model with lipid pool, D) Deflation for Ogden N1 material model with lipid pool, E) Max inflation for Ogden N1 material model with calcifications and F) Deflation for Ogden N1 material model with calcifications.

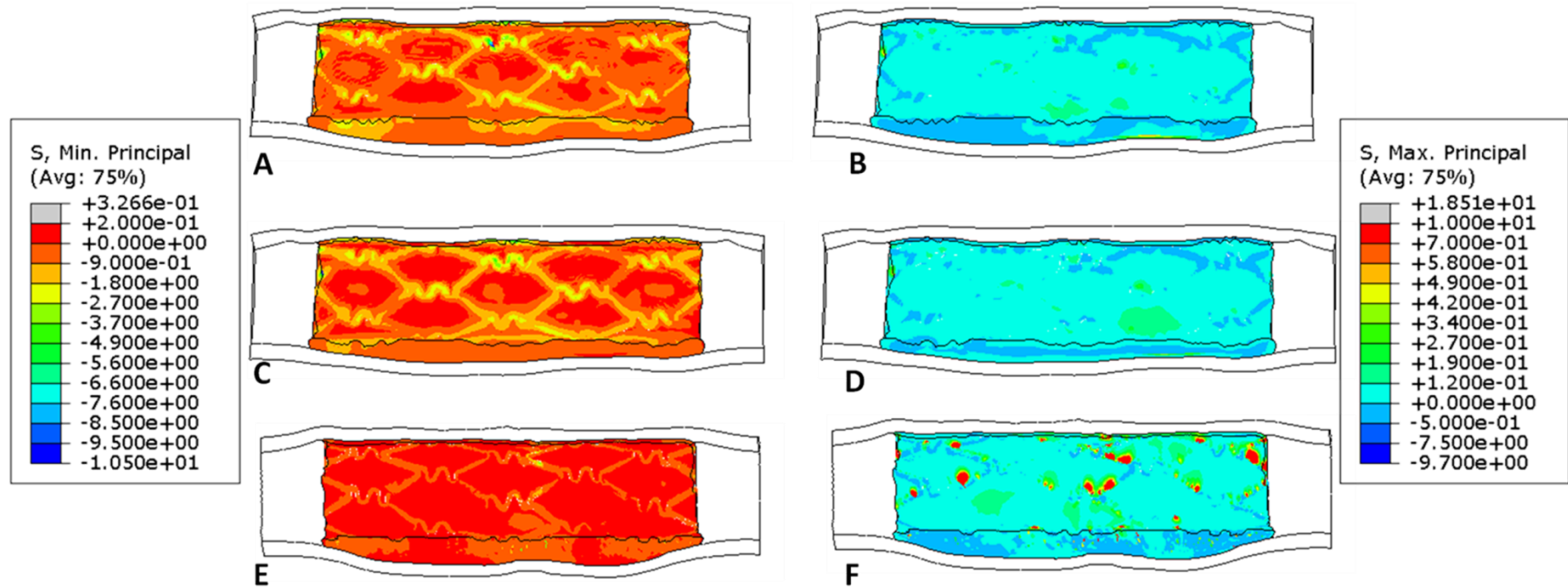


Figure 8 Principal stress distribution (MPa) in atherosclerotic tissue at maximum balloon inflation, A) Minimum principal stress for Ogden N1 material model, B) Maximum principal stress for Ogden N1 material model, C) Minimum principal stress for Ogden N1 material model with lipid pool, D) Maximum principal stress for Ogden N1 material model with lipid pool, E) Minimum principal stress for Ogden N1 material model with calcifications and F) Maximum principal stress for Ogden N1 material model with calcifications.